ingegneria sismica
International Journal of Earthquake Engineering
Anno XLIII - Num. 2 - 2026

Fracture and crack resistance of high-performance fiber-reinforced concrete

Cuijin Wang[1,*]

[1] Department of Civil and Environmental Engineering, Chengdu Jincheng College, Chengdu, Sichuan, 611731, China

SUMMARY: *Concrete is among the most adaptable materials. However, it has a tendency to crack due to its inherent properties, low strength, poor toughness and other defects, thus limiting its application in large buildings and some special buildings. The present paper carries out a discussion regarding the influence of high-performance fiber-reinforced concrete upon fracture performance. We carry out the analysis of the microscopic cracking characteristics of the specimen by means of utilizing the finite element numerical simulation method.The fracture characteristics of the specimen, including fracture energy, fracture toughness, and critical tensile displacement, were computed. After that step, an evaluation was carried out to confirm the influences of the maximum aggregate size, steel fiber length, and volume ratio on the crack expansion process and breaking energy of steel fiber-reinforced concrete.The findings indicate that as the level of material integrity impairment increases, the proportion of shear microcracks in the total number of cracks rises. Different types of fiber concretes exhibited significant differences in fracture toughness at conventional fiber admixtures. When making contrast with common concretes and PVA-fiber concretes, the load-deflection curves of steel-fiber and ternary blended-fiber concretes are more full and round, and they show very good fracture toughness. The proceeding of crack expansion inside steel fiber-reinforced concrete was obviously influenced by three elements: the maximal dimension of coarse aggregates, the longness of steel fibers, and the volume percentage of steel fibers.*

KEYWORDS: *fiber concrete; fracture properties; extended finite element method; numerical simulation*

1 Introduction

Concrete is an inhomogeneous, discontinuous multiphase composite material with high brittleness. This brittleness makes it have many fatal drawbacks in terms of shrinkage, flexural and tensile resistance, toughness, etc., which bring a lot of unfavorable and potential dangers to the project [1]. Consequently, since the existence of cement concrete, the crack problem has been plagued by people, many scholars and experts attempted to solve the shrinkage cracks from different ways to enhance the toughness of concrete, so far the compensation shrinkage concrete mixed with expansion agent in the building seepage and crack resistance of the research and application of more [2]. Engineering practice has also proved that general commercial concrete mixed with fly ash plus pumping agent or commercial concrete mixed with expansion agent has some effect on concrete crack control. However, due to construction, maintenance and human factors, concrete casting cracks are still inevitable. So far scholars in

*elizabethwangcj@163.com
https://doi.org/10.65102/is2026573
Published: 30 April, 2026

various countries put the target to fiber, the use of fiber reinforced toughened cement concrete has attracted extensive attention from researchers [3].

In the passed several years, research workers coming from various countries have brought out the opinion of mixing fibers into concrete. This adding work is designed to give concrete a certain degree of tenacity, hence strengthening its capability to withstand crack emergence, and made a lot of practical research. Steel fiber concrete is a new type of multi-phase composite material formed by mixing short steel fibers distributed in a chaotic manner in ordinary concrete. The tensile, flexural and shear strengths of steel fiber concrete have been effectively improved compared to ordinary concrete [4]. Take as example, Abbass and his cooperative researchers have investigated how steel fibers with different lengths and diameters influence the mechanical properties of concrete that belongs to three different strength classes. They have found that adding steel fibers can greatly improve the mechanical performances of concrete.Concretely speaking, the compressive strength had a growth of about 10-25%, furthermore, the direct pulling strength has beheld an approximate increase of 31 to 47 percentage[5]. Niu and his workmates conducted an investigation on the expanding behavior of cracks inside common steel fibers of diverse lengths that exist inside ultra-high performance concrete. The entire mixing amount is stipulated to 2.0%, and the substitution proportions are set as 0.5%, 1.0%, and 1.5%. This research was carried out by way of bending load experiments[6].Yao and his collaborators worked out a design method for the fracture characteristics of steel fiber-reinforced concrete. This research method considers the combined effect that is exerted by the natures of steel fibers and the distribution of aggregate grain dimensions.We must point out that there exists only the requirement for one kind of sample and one testing standard. When it is combined with input data which are like the characteristic parameters of steel fibers, the characteristic particle size of the aggregate, the peak static load, and the specimen dimensions, therefore it becomes possible that we can simultaneously determine the fracture toughness and tensile strength of steel fiber-reinforced concrete [7]. Luo and his workmates made high-function concrete strengthened by steel fibers through a compound craft that unites mortar infiltration and vibration, and found that its peak compressive strength reached 140 MPa and peak flexural strength reached 80 MPa, which were 61% and 774% higher than that of the unreinforced hardened mortar, respectively, with a flexural compressive strength ratio of 0.6, and the damage mode showed pseudo-plasticity characteristics of multi-cracking development [8].

Glass fiber, a high - performing inorganic non - metallic substance, exhibits remarkable resistance to corrosion, flexural, tensile and other high-quality performance,therefore, the adding of glass fiber into concrete can greatly promote the total performance of the concrete.Within the glass fiber - reinforced concrete, the glass fibers integrate effectively with the cementitious mortar to create a functional "fiber lattice". This lattice serves to enhance the concrete's resilience and stifle the propagation of existing cracks as well as the appearance of fresh ones. [9]. Wu and colleagues conducted experiments to study the influence of alkali-resistant glass fiber addition, which is from 0.0% to 1.5%, on the mechanical properties and micro-structure of concrete; it was found that the encapsulation of fibers by the slurry weakened with the increase of fiber admixture; and the energy spectral analysis confirmed that the moderate amount of fiber admixture did not affect the hydration reaction of cement [10].Aliha together with his work partners have carried out research on the effect which 72 different proportions have on the Type I fracture performance of polymer concrete. These proportionals include epoxy resin which lies between 17% and 25%, coarse with fine aggregates which range from 75% to 81%, and 0 - 2% short-cut E glass fibers. We have carried out the investigation through semicircular bending fracture experiments [11]. Xiaochun together with workmates carried out research on the corrosion mechanism and performance of alkali-resisting glass fibers

which are inside cement mortar. They moreover have carried out an examination on whether these fibers possess the suitability to be applied in the concrete of road ways. Their research results showed that mixing 30% fly ash or 10% silica fume can greatly promote the capacity of the cement base body to safeguard the alkali-resistant glass fibers against corrosion [12]. Zhang and his work group used perpendicular design and experiments to make sure the best mixture of alkali-resisting glass fiber quantity and its influence to concrete strength. In addition, they have carried out an analysis upon the micro-structure by making use of SEM images. This analysis has discovered the connection between the micro structure and macro properties, and it has also made clear the mechanisms of strength increasing and crack resisting.In the end, a digital calculation model of randomly scattered fiber-enhanced cement concrete was hence established. After that, by means of finite element simulation, the development characteristics of alkali-resistant glass fiber concrete under stretching damage were investigated [13]. Ruben and his professional team have carried out an all-around evaluation on the serviceability of glass fiber-reinforced concrete within the domain of structure engineering.They reached this result through carrying out one group of experiments, for example slump, split-tension, compressive-flexure, chloride ion penetration, and accelerated corrosion experiments. This process has the span that starts from the investigations which are based in laboratory, and hence goes to the industrial applications which are in the real world. In addition, they did implement SEM and EDS microanalysis works to obtain a more deep-going comprehension [14].

On account of their noteworthy tensile intensity, great tenacity, and money saving advantage, polypropylene fibers were joined into concrete by appropriate amounts. This adding operation was implemented to greatly promote the concrete's capacity for bearing compression and opposing cracking.Latifi and colleagues demonstrated via their analysis that the integration of polypropylene fibers boosts the concrete's durability against abrasion as well as freezing and thawing cycles. Moreover, it diminishes the volumetric expansion resulting from sulphate erosion and the alkali - silicic acid reaction. Additionally, the inclusion of these fibers improves the concrete's capacity to endure energy dissipation. It also substantially lessens plastic shrinkage cracking, which improves durability and reduces whole life cost [15]. Liu and his working team have carried out an all-round summary discussion about the influences that polypropylene fibers bring to the many-sided endurance performance features of concrete. These performance properties include dry contraction, creep deformation, water absorption, permeation ability, anti-chloride penetration ability, anti-sulfate erosion ability, anti-freeze-thaw cycle ability, carbonization resistance ability, and fire resistance ability. They also have done the examination on the action mode of the fiber mixture, together with the effect from fiber diameter and mixing proportion [16]. Qin and his research team have carried out an investigation into the feasibility of using waste polypropylene fiber textiles as a strengthening material for concrete.They did execute experiments to make specimens from spunbonded polypropylene materials that come from cast-off clothes. The putting of waste fiber cloth materials into the concrete can promote the compressive performance of concrete and its energy absorbing ability[17]. Alsadey and Salem have carried out one group of systematic experiments for inspecting the influence that polypropylene fiber admixture brings to the compressive strength of M25 grade concrete. The experiment results told us that along with the increment of the fiber admixture's quantity, the concrete's compressive strength had a significant promotion. Specially, when the fiber addition amount has achieved 2%, a obvious increasing has been observed. The 28-day press resistant intensity of the concrete on this level was 28 N/mm², it approximately represents a 12% raise when compared with the control group [18]. Ibrahim and his workmates prepared nine groups of concrete which is strengthened by polypropylene fiber. The fiber volume adding content in these test groups changed from 0.06% to 2.16%. Research workers have found that when the percentage of fiber that is mixed into

concrete is about 0.36%, the 28-day compressive strength, splitting tensile strength, and flexural strength of concrete all reach their peak values. But, when the amount of added fiber is more than 0.36%, the too great number of fiber interfaces will bring about a lowering of the binding power inside the substrate and the processing performance of the concrete. Therefore, the intensity of the concrete has a decrease[19].

Natural fiber - incorporated concrete is a type of composite substance made by blending natural fibers into regular concrete, which has good performance and environmental advantages. Krishna et al. selected coconut fiber and sisal fiber as natural reinforcing materials to improve the performance of concrete, and focused on exploring the optimal amount of coconut fiber to enhance the ductility of concrete by using plain concrete as a benchmark, and to carry out the assessment of the influence that sisal fiber exerts on the strength characteristics of concrete through the examination of the reinforcing action of sisal fiber upon these strength properties [20]. Islam and Ahmed conducted an assessment of how jute fibers impact the workability and hardening characteristics of concrete. TThese researchers have discovered that a proper quantity of jute fibers is able to promote the compressive, splitting tensile, and flexural strength of concrete. This result provides a experiment basis for the development of environment-protective fiber-reinforced concrete [21]. Ahmadi and his work companions found that adding recycled steel fibers which come from waste into recycled aggregate concrete can obviously promote its mechanical performance properties. This method enables concrete that has a 50% recycled aggregate replacement rate to satisfy the strength standard that is required for structural concrete. Furthermore, the incorporation of fibers can effectively bring about the reduction of the thickness of the concrete road surface. To speak specifically, a 0.5 percent fiber adding component leads to an approximately 8 percent cut in thickness, while a 1 percent adding component brings about about a 16 percent lowering [22]. Geremew and colleagues determined that integrating natural fibers into concrete necessitates enhancing their interfacial bond with the polymer matrix. This can be achieved via physical, chemical, or biological surface - treatment methods. The reason for this is that natural fibers offer the benefit of being readily accessible,renewable, biodegradable, low-cost, low-density, and excellent specific properties [23]. A research conducted by Ahmad and his colleagues revealed that jute fibers can improve the robustness and longevity of concrete, but reduce the flowability of fresh concrete, and its mechanism of action is similar to that of synthetic fibers, furthermore, the perfect mixing ratio generally lies between 1% and 2%, which is dependent on the length and the diameter that the fibers have.[24]. Yinh et al. found that incorporating natural sisal fiber-reinforced composites into reinforced concrete members can improve their strength and performance, and proposed a novel anchoring system that effectively prevents the problem of easy delamination of natural sisal fiber-reinforced materials [25].

Basalt fibers are continuous thread-shaped things which get from natural basalt. Very many research studies have already proven that mixing basalt fibers into concrete can raise the concrete's stretching strength, anti-impact performance, capacity for bearing cracking, and water-proof ability[26]. Zhou and his work companions have carried out assessment on the hardness and crack performance features of concrete which is reinforced by fiber. They utilized fracture energy, which is one kind of advanced toughness parameter, and Hillerborg characteristic lengths to carry out this evaluation. After that step, they brought in fiber correlation coefficients to constitute a computation formula for mechanical properties. This formula gives a quantitative base for the design and use of basalt fiber-reinforced concrete [27].Branston and his work colleagues conducted a contrast on the strengthening effects of two different kinds of basalt fibers, that is bundled scattered fibers and tiny rods, for the mechanical properties of concrete. They found that two types of basalt fibers all enhanced the pre-cracking intensity of concrete. But, it is only the micro rods that have the enhancement on the behavior

after cracking takes place. This enhancement was attributed to the promotion of the fiber-substrate contact surface characters by its polymer protection layer [28]. Jalasutram et al. explored the effect of short-cut basalt fiber admixture (0-2%) on the mechanical properties of fiber-reinforced concrete, and found that the addition of fibers slightly reduces the compressive strength of concrete, however, it has the ability to shift its damage pattern from a brittle state to a ductile one. This occurs when the proportion of fiber admixture attains 2%, the splitting tensile strength of the concrete is enhanced by about 15%, the flexural strength is significantly increased by up to 75%, and the post-peak residual strength improved significantly [29]. Khan and colleagues employed scanning electron microscopy analyses to uncover the crack - resistant mechanisms and the interactions at the interface between basalt fibers and the matrix. Based on these findings, they put forward the HyFRC stress - strain analysis model. This model showed a high degree of consistency with the experimental data, as indicated by an R^2 value of 0.92 or higher. This result validates the potential of basalt fibers of varying lengths and with different admixtures in enhancing the multi - layered characteristics of concrete[30].

The present research mainly uses ABAQUS finite-element software to study the fracture and crack-resistance performances of steel-fiber-reinforced concrete.Furthermore, it has the formulation of the inherent model, bonding break model, and finite-unit model of steel-fiber-enhanced concrete. First, we have carried out one examination on the micro fracture mode of steel fiber added concrete and its connected characteristics.Subsequently, numerical simulations were carried out using plain concrete, polyvinyl alcohol (PVA)-added concrete, regular steel fiber - reinforced concrete, ultra - fine steel fiber - reinforced concrete, and multi - fiber concrete, which was a blend of these three materials. The purpose of these simulations was to explore the variations in fracture toughness among different kinds of fiber - reinforced concrete. Finally, the effects of maximum coarse aggregate size, steel fiber length and steel fiber volume rate on the fracture and cracking resistance of steel fiber concrete were analyzed.

2 Three-dimensional detailed modeling of high-performance steel-fiber concrete

In this research paper, we take steel fiber-reinforced concrete as the concrete object of our study. We have built a model for steel fiber-reinforced concrete which is based on ABAQUS software. To every composition part of the inside materials, one suitable constitution model has been chosen by us. The performance features of material have been given accurate definitions, and the grid has been carried out division. After that, the fracture behavior is through the simulation of a three-point bending test to be studied.

2.1 ABAQUS finite element software

ABAQUS software is a full-featured large-scale finite element software, ABAQUS software internal not only includes static, quasi-static analysis and fracture analysis, but also includes coupling analysis, mass diffusion analysis. The software internal mainly includes three modules: The ABAQUS/CAE processing module encompasses two analysis modules: ABAQUS/ Standard and ABAQUS/Explicit.

The process of simulation and analysis using ABAQUS software is shown in Figure 1, which is mainly divided into three steps, in which the pre-processing is mainly using ABAQUS/CAE processing module for the establishment of the model, as well as the need for some parameter definitions and so on. Numerical calculation is based on the problem we want to analyze corresponding to the choice of the appropriate solver, or a combination of two solvers for simulation and analysis of the calculation. Post-processing is performed using

ABAQUS/view, a sub-module of the ABAQUS/CAE Processing Module, for post-processing the results, including efficient plotting.

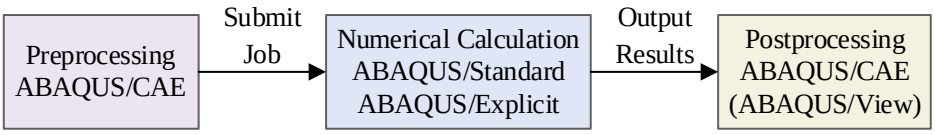

Figure 1: ABAQUS simulation analysis process

2.2 Ontological modeling

2.2.1 Mortar principal modeling

Within the ABAQUS finite - element software, three types of constitutive models exist for concrete materials: the dispersed cracking model, the brittle fracture model, and the plastic impairment model.

In this research paper, we regard mortar as one kind of concrete which does not have coarse aggregate. With respect to the built-in model of mortar, we utilize the concrete damage plasticity model (CDP model) which is included in the ABAQUS software. The CDP model may be utilized in the Standard and Explicit modules of ABAQUS as well. Up to present, it is the model that gets the widest utilization for concrete materials. This model brings in damage variables to describe the cracking process of concrete when it bears load. It achieves this function by means of an isotropic elastic and tension-compression plastic damage method. This model includes two different damage mechanisms. The first problem is concrete occurrence of cracking when it is suffered from tensile stress, and the second problem is concrete occurrence of crushing when it is under compressive stress.

Among them, the stress-strain curve of concrete when subjected to uniaxial compression can be calculated and determined by Eqs. (1) to (5):

$$\sigma = \left(1 - d_c\right) E_c \varepsilon \tag{1}$$

$$d_c = \begin{cases} 1 - \dfrac{\rho_c n}{n - 1 + x^n}, & x \le 1 \\ 1 - \dfrac{\rho_c}{\alpha_c \left(x - 1\right)^2 + x}, & x > 1 \end{cases} \tag{2}$$

$$x = \frac{\varepsilon}{\varepsilon_{c,r}} \tag{3}$$

$$\rho_c = \frac{f_{c,r}}{E_c \varepsilon_{c,r}} \tag{4}$$

$$n = \frac{E_c \varepsilon_{c,r}}{E_c \varepsilon_{c,r} - f_{c,r}} \tag{5}$$

where d_c is the uniaxial compressive damage evolution parameter, E_c is the modulus of elasticity, and $f_{c,r}$ is the representative value of uniaxial compressive strength. $\varepsilon_{c,r}$ is the

peak compressive strain, calculated as $\varepsilon_{c,r}=\left(700+172\sqrt{f_c}\right)\times 100^{-6}$. α_c is the parameter value of the descending section of the stress-strain curve under uniaxial compression, calculated as $\alpha_c=0.157\,f_c^{0.785}-0.905$.

The stress-strain curve under uniaxial tension can be determined by equations (6) to (9):

$$\sigma=\left(1-d_t\right)E_c\varepsilon \tag{6}$$

$$d_t=\begin{cases}1-\rho_t\left[1.2-0.2x^5\right], & x\le 1\\ 1-\dfrac{\rho_t}{\alpha_t\left(x-1\right)^{1.7}+x}, & x>1\end{cases} \tag{7}$$

$$x=\frac{\varepsilon}{\varepsilon_{t,r}} \tag{8}$$

$$\rho_c=\frac{f_{t,r}}{E_c\varepsilon_{t,r}} \tag{9}$$

where: d_t is the uniaxial tensile damage evolution parameter and $f_{t,r}$ is the representative value of uniaxial tensile strength. $\varepsilon_{t,r}$ is the peak tensile strain, calculated as $\varepsilon_{t,r}=f_{t,r}^{0.54}\times 65\times 10^{-6}$. α_t is the parameter value of the descending section of the stress-strain curve under uniaxial tension, calculated according to $\alpha_t=0.312\,f_{t,r}^2$.

The stress - strain curves for uniaxial compression and uniaxial tension can be acquired as depicted in Figure 2 through Figure 3.

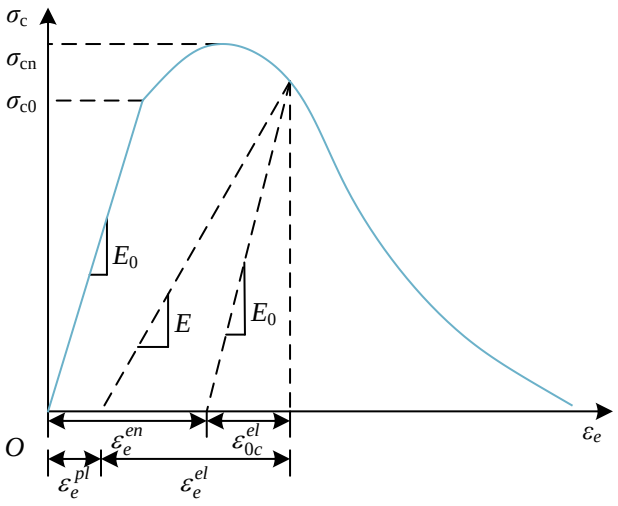

Figure 2: Uniaxial compression stress-strain curve

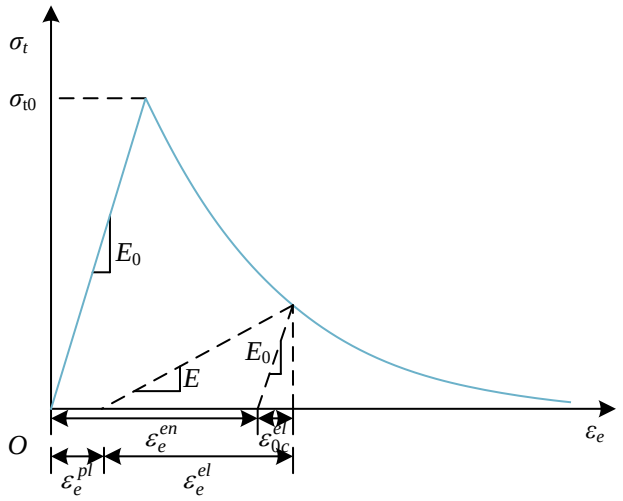

Figure 3: Uniaxial tensile stress-strain curve

This paper simulates the three-point bending test, so it mainly discusses the constitutive relationship after the tensile concrete reaches the peak stress, while for the compressive constitutive, this paper carries out a simplified treatment.

Figure depicts the stress - strain curve of mortar when it undergoes tensile damage. 3, and the total strain is decomposed into two parts, elastic strain and plastic strain, with the following expressions:

$$\varepsilon_t = \varepsilon_t^{pl} + \varepsilon_t^{el} \tag{10}$$

$$\sigma_t = (1-d_t) E_0 \left(\varepsilon_t - \varepsilon_t^{pl}\right) \tag{11}$$

$$E = (1-d_t) E_0 \tag{12}$$

where: ε_t is the total strain, ε_t^{pl} is the plastic strain, ε_t^{el} is the stress at the effective elastic modulus, d_t is the damage variable, and E_0 is the modulus of elasticity that this represents when the undamaged condition is reached.

The stress expression after entering the softening stage is:

$$\sigma_t = (1-d_t) E_0 \left(\varepsilon_t - \varepsilon_t^{pl}\right) \tag{13}$$

The expression for effective stress is as follows:

$$\bar{\sigma}_t = \frac{\sigma_t}{(1-d_t)} = E_0 \left(\varepsilon_t - \varepsilon_t^{pl}\right) \tag{14}$$

The direct use of Eq. (14) in the simulation analysis will inevitably increase the sensitivity of the results to the mesh. When the material strain ε reaches the ultimate strain ε_u the material begins to break down. Assuming that the dimensions of the cell are L, the deformation u of the material at this point is:

$$u = L \times \varepsilon_u \tag{15}$$

Through the inspection of the above-mentioned equation, we can find that when the volume of the cell becomes larger, the corresponding deformation therefore also becomes larger, the larger the overall displacement, and vice versa. This suggests that the use of $\sigma-\varepsilon$ curves to characterize material damage leads to mesh-dependent results. Therefore, in this paper, the fracture energy G_f proposed by Hillerbog is introduced to characterize the stress as a function of the cracking displacement.

The curve in Fig. 3 is simplified, i.e., the rising section is regarded as a straight line, while for the falling section, an exponential function is used to express the corresponding stress-strain curve expression:

$$\begin{cases}\sigma_t = E_0\varepsilon, \varepsilon \le \varepsilon_{tu} \\ \sigma_t = \sigma_{tu} e^{-A(\varepsilon-\varepsilon_{tu})}, \varepsilon > \varepsilon_{tu}\end{cases} \tag{16}$$

where: E_0 is the modulus of elasticity in the nondestructive state, σ_{tu} is the peak stress, ε_{tu} is the peak strain corresponding to the peak stress, and A is the control factor.

The effective stress may be expressed in this way:

$$\begin{cases}\bar{\sigma}_t = E_0\varepsilon, \varepsilon \le \varepsilon_{tu} \\ \bar{\sigma}_t = \sigma_{tu}, \varepsilon > \varepsilon_{tu}\end{cases} \tag{17}$$

The injury variable is denoted as:

$$d_t = 1 - \frac{\sigma_t}{\bar{\sigma}_t} \tag{18}$$

When the material enters the softening stage, the total strain is decomposed into peak strain and cracking strain, and the corresponding expressions are as follows:

$$\varepsilon = \varepsilon_{tu} + \varepsilon^{ck} \tag{19}$$

Simultaneous multiplication of both sides of Eq. (19) by the cell size L yields a decomposition curve for the displacement with the expression:

$$u = u_0 + u^{ck} \tag{20}$$

Let $A = B \cdot L$, which is collapsed by substituting it into Eq. (16):

$$\begin{aligned}\sigma &= \sigma_{tu} e^{-BL(\varepsilon-\varepsilon_{tu})} = \sigma_{tu} e^{-B(\varepsilon L-\varepsilon_{tu} L)} \\ &= \sigma_{tu} e^{-B(u-u_0)} = \sigma_{tu} e^{-Bu^{ck}}\end{aligned} \tag{21}$$

According to the fracture energy concept, integrating over the cracking displacement u^{ck} for σ_t yields:

$$G_f = \int_0^{+\infty} \sigma_t du^{ck} = \frac{\sigma_{tu}}{B} \tag{22}$$

For the same material, both G_f and σ_{tu} are material constants, so B is also a material constant.

Bringing Eq. (22) into Eq. (21) and Eq. (18), the stress-displacement ontological relationship and damage variables for the softening stage can be obtained:

$$\sigma_t = \sigma_{tu} \times e^{-\frac{\sigma_{tu}}{G_f} u^{ck}} \tag{23}$$

$$d_t = 1 - e^{-\frac{\sigma_{tu}}{G_f} u^{ck}} \tag{24}$$

Eqs.The employment of stress - cracking displacements to depict the plastic damage inherent model, spanning from (23) to (24), eliminates the correlation between stress - strain and mesh size. As a result, it diminishes the simulation's susceptibility to the mesh.

2.2.2 Aggregate principal modeling

In the process of actual testing, when the test piece breaks, there appears a situation in which the aggregate undergoes failure. Therefore, inside this paper, the aggregate is regarded as an ideal elastic-plastic body. In other words, the aggregate material possesses its own final strength which is ultimate. When this intensity is exceeded in the loading process, therefore, the aggregate loses its function.

2.2.3 Fiber principal model

Steel fiber, that belongs to the category of metallic materials, is in its essence one kind of steel. Therefore, the tensile intensity of steel fiber is obviously larger than that of the base body. When a steel-fiber concrete test piece bears damage and breakage, the steel fibers are in the main pulled out. For them, the situation that they break rather than get pulled out is an extremely rare occurrence. Therefore, for the purpose of matching the actual situation in real world, this paper does not make consideration of the destruction that comes from steel fibers. On the contrary, the steel fibers shall be employed in accordance with the principal relation of linear elasticity.

2.3 Cohesive crack modeling

2.3.1 Basic Ideas

Five primary categories of finite element models are employed to mimic the cracking behavior of concrete. These include the smeared crack model (SCM), the distinct crack model (DCM), the fracture mechanics - based model (FMM), the crack model which is based on the extended finite element method (XFEM) and the cohesive crack model (CCM).

In this paper, the bending experiments use the cohesiveness crack model to carry out simulation and analysis for the crack behavior of steel fiber-reinforced concrete composite materials.The basic idea of the cohesive crack model is to embed a layer of cohesive units in a solid unit, which describes the generation, expansion and evolution of cracks under loading. The basic connection of the cohesive crack model is established on the basis of the traction-separation idea, the damage starting idea, and the damage development idea.

2.3.2 Traction-Detachment Criteria

The bilinear simplified model of the traction-separation criterion is shown in Fig. 4. The traction-separation behavior consists of two parts, the line elastic branch and the softening

branch. The traction force F in the line elastic branch region increases linearly with the increase of the tensile displacement,in addition, the slope of the curve may be described as the starting stiffness of the testing sample.The slope of the curve can be defined as the initial stiffness of the test specimen. Until the maximum traction force $T_{\max}$ is reached, which means that the damage starts, the tension displacement keeps increasing while entering into the softening branch, the traction force T shows a decreasing tendency along with the increase of the tension displacement, until finally the traction force T drops to 0 marking the cohesive crack formation. When we talk about a bending structure member, the direction that the crack grows in is a right angle to the direction that the principal stress lies in,and the crack makes the traction force T form a functional relationship with the tensile displacement δ during the evolution process, which can be defined as:

$$T = f(\delta) \tag{25}$$

The area enclosed by the traction force F and the tensile displacement δ is the fracture energy G^C, which follows:

$$G^C = \int T d\delta \tag{26}$$

We use the cohesive fracture model to carry out the description of the fracture behavior of composite materials, with T_0 denoting the original thickness of the intrinsic unit, so the nominal strain can be defined as:

$$\varepsilon_n = \frac{\delta_n}{T_0}, \varepsilon_s = \frac{\delta_s}{T_0}, \varepsilon_t = \frac{\delta_t}{T_0} \tag{27}$$

Subsequently, the matrix representation of the elastic eigenstructure for the traction - detachment behavior can be presented as follows:

$$t = \begin{Bmatrix} t_n \\ t_s \\ t_t \end{Bmatrix} = \begin{bmatrix} E_{nn} & E_{ns} & E_{nt} \\ E_{ns} & E_{ss} & E_{st} \\ E_{nt} & E_{st} & E_{tt} \end{bmatrix} \begin{Bmatrix} \varepsilon_n \\ \varepsilon_s \\ \varepsilon_t \end{Bmatrix} \tag{28}$$

where t_n is the normal stress, t_s and t_t are the tangential stresses, ε_n is the normal stress, ε_s and ε_t are the tangential stresses, and E is the elasticity matrix of the cohesive unit.

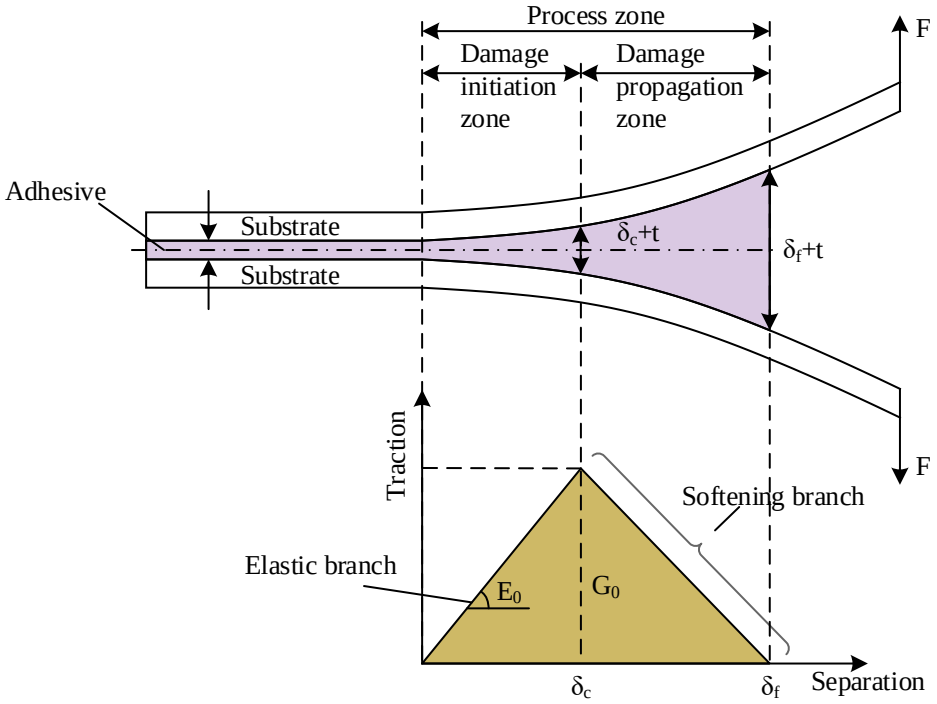

Figure 4: Bilinear simplified model of the traction and separation criterion

2.3.3 Injury initiation criteria

The occurrence of damage has connection with the beginning of the decline of composite material function. In this research paper, we utilize the Quads Damage quadratic nominal stress criterion which is provided by ABAQUS. This standard defines that damage starts at the point where the sum of the squares of the nominal stress ratios in all directions is equal to one. It is namely:

$$\left\{\frac{t_n}{t_{n(\max)}}\right\}^2+\left\{\frac{t_s}{t_{s(\max)}}\right\}^2+\left\{\frac{t_t}{t_{t(\max)}}\right\}^2=1 \tag{29}$$

where $t_{n(\max)}$, $t_{s(\max)}$ and $t_{t(\max)}$ the nominal stress peak values in the normal direction,the peak numerical values of the nominal stress in the starting tangential direction, and the nominal stress peak values in the second tangential direction.

2.3.4 Damage Evolution Criteria

The onset of damage evolution is signaled by the cohesive stress reaching the maximum stress criterion, and a damage variable d is introduced here to describe this degraded state. The relationship between the post-damage stress t and the no-damage stress t_E is:

$$t=(1-d)t_E \tag{30}$$

The damage variable d contains the combined effect of all damage mechanisms, and d increases monotonically from 0 to 1, leaving the material undamaged when $d=0$ and completely damaged and destroyed when $d=1$.

The damage evolution is based on either energy or displacement. Regarding the cohesion

ontology relationship founded on displacement - based damage progression, it is necessary to give the maximum nominal stress or displacement δ_m corresponding to the beginning of damage evolution and the maximum displacement δ_m^f corresponding to complete damage destruction, and for the linear form of damage evolution, the damage variable d can be expressed as:

$$d = \frac{\delta_m^f \left(\delta_m^{\max} - \delta_m\right)}{\delta_m^{\max} \left(\delta_m^f - \delta_m\right)} \tag{31}$$

With respect to the exponential form that damage develops, the damage variable can be expressed in the following way:

$$d = 1 - \left\{\frac{\delta_m^0}{\delta_m^{\max}}\right\}\left\{1 - \frac{1 - \exp\left(-\alpha\left(\frac{\delta_m^{\max} - \delta_m^0}{\delta_m^f - \delta_m}\right)\right)}{1 - \exp(-\alpha)}\right\} \tag{32}$$

where α denotes the rate of damage evolution.

The use of linear energy based damage evolution requires the fracture energy to be given, which can be defined as using the Benzegah-Kenane (BK) analytical equation:

$$G^C = G_n^C + \left(G_s^C - G_n^C\right)\left\{\frac{G_s}{G_T}\right\}^{\eta} \tag{33}$$

With respect to the exponential pattern of damage development, the damage variable can be expressed in the following way:

$$d = \int_{\delta_m^0}^{\delta_m^f} \frac{T_{eff}\, d\delta}{G^C - G_0} \tag{34}$$

$$\delta_m^f = 2G^C / T_{eff}^0 \tag{35}$$

$$T_{eff} = \sqrt{\{t_n\}^2 + t_s^2 + t_t^2} \tag{36}$$

where G^C is the total fracture energy. G_n^C and G_s^C are the normal and tangential fracture energy, respectively. G_n is the normal-to-variable energy release rate. G_s and G_t are the two tangential strain energy release rates. η is the material parameter. T_{eff}^0 is the traction force at the beginning of the damage. G_0 is the elastic energy at the onset of damage.

2.4 Construction of Finite Element Model

2.4.1 Model description

The flexural mechanical characteristics of steel fiber - reinforced concrete composites are

examined via numerical simulation with the large - scale finite element software Abaqus/Explicit. The whole bending finite element model is shown in Fig. 5, which consists of three parts: Part-concrete, Part-steel fiber and Part-rigid body indenter and support.

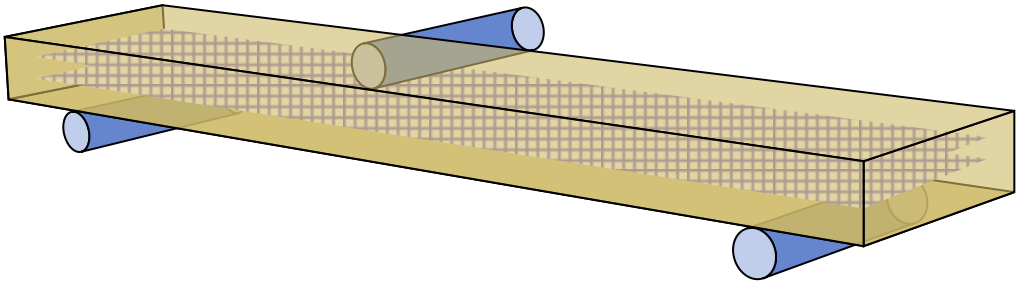

Figure 5: Bending finite element model of steel fiber reinforced concrete composite materials

2.4.2 Analytical steps and contacts

The entire finite element simulation presents only bending behavior, so only one analysis step, Step-1, is set up. The bending simulation is geometrically nonlinear, and the Nolinear Geometry is always “On” throughout the entire calculation process. In order to ensure the successful cracking of the cohesive unit, it is necessary to set the field variables to SDEG and DMICRT in Failure/Fracture and STATUS in State/Field/User/Time, and the indenter and support do not undergo any deformation throughout the entire numerical simulation. The size of the mass does not affect the convergence and the final simulation results. In order to guarantee that there exists no sliding displacement between the rigid-body pressure head, the supporting base, and the concrete material, the interactive action among them is constructed by utilizing the “Tie” binding connection. The outer side face of the top pressure head and the top face of the concrete are disposed by means of the discrete "Surface to Surface" method. This same separate “Surface to Surface” approach is utilized to establish the connection between the outer face of the upper pressing head and the top face of the concrete. The concrete's below face is split into two sections and fixed with the bottom support. The mutual touch between the steel fibers and the concrete is stipulated through the "Embedded region". This definition takes the precondition that there does not exist relative sliding between the units.

2.4.3 Loads and Boundary Conditions

In the numerical simulation of steel fiber-reinforced concrete composite materials, the pre-given velocity field is used as the loading mode for applying boundary conditions, considering the force characteristics of bending properties and the bearing process of structural members, the translational degree of freedom and rotational degree of freedom of steel fibers and concrete should not be restricted, and the load and boundary control are mainly applied to the indenter and the support. The load and boundary control of the finite element model are shown in Fig. 6, with U1, U2 and U3 denoting the translational degrees of freedom in the three directions, UR1, UR2 and UR3 denoting the rotational degrees of freedom in the three directions, and V3 denoting the translational velocity in the Z direction. Regarding the lower support, all translational and rotational degrees of freedom are restricted and held stationary. As for the upper indenter, the translational degrees of freedom along the X and Y axes, as well as the rotational degrees of freedom around the X, Y, and Z axes, are constrained and immobilized. In accordance with the loading speed planned for the test, a translational speed of -3 mm/min is applied in the Z - axis direction. Here, the negative sign indicates the direction.

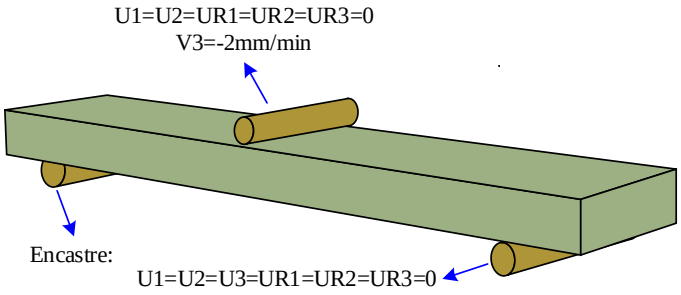

Figure 6: Load and boundary control of the finite element model

2.4.4 Grid division

The grid division possesses an influence on the convergence of the computation and the time-related effectiveness of the analysis. This diagram displays the grid division of the finite-element model. In this situation, the concrete net is divided by the C3D8R reduced integration unit type. The advantage of this kind of cell is that the cell's shape exerts the minimal influence upon the final results of numerical simulation. Furthermore, the mesh partition method that we use is the sweeping division method.The steel fiber mesh is divided by B31 linear beam cell type, and the mesh division technique also adopts swept division. The upper compression head and lower support rigid body meshing adopts R3D4 bilinear rigid quadrilateral cell type, and the meshing technique adopts free division. The cohesive cracks are meshed using COH3D8 3D cohesive cell type.

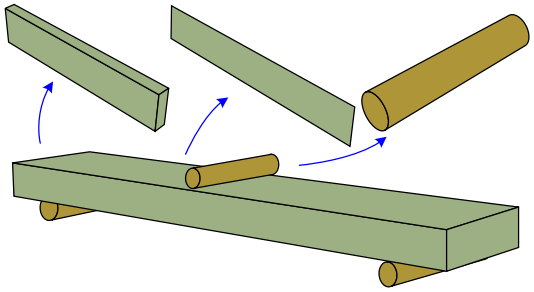

Figure 7: Meshing of the finite element model

3 Model simulation analysis

In this particular chapter, the Abaqus software is employed to construct a three - dimensional model of steel fiber - reinforced concrete. Subsequently, by conducting microscopic cracking analyses and numerical simulations, the fracture damage mechanism of steel fiber - reinforced concrete is explored. The aim is to find out the factors which give influence and the basic rules which control the fracture mechanics features of concrete that is reinforced by steel fibers.

3.1 Microcracking analysis

The acoustic emission waveform schematic and basic parameters are shown in Fig. 8, i.e., count (C_{AE}), amplitude (A_{AE}), rise time (RT), and duration (DUR). Studies have shown that, compared with the tensile cracking mode, the rising time of the acoustic emission waveform in the shear cracking mode is longer and the amplitude is lower. Therefore, the average frequency AF (i.e., C_{AE} / DUR) and the cotangent of the inclination angle RA (i.e., RT / A_{AE}) are

often used to determine the cracking mode of micro-cracks in steel fiber concrete materials. The ratio AF / RA (referred to as the AR value) is used for this purpose. That is, when the AR value is larger, it indicates a tensile cracking mode signal, and when it is smaller, it indicates a shear cracking mode signal. The AR_{lim} in the figure is the critical value for distinguishing between tensile and shear cracking modes.

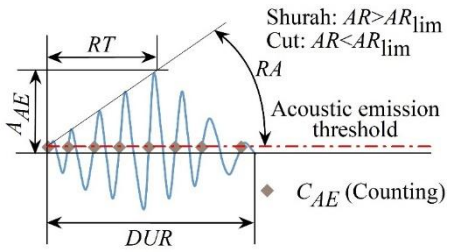

Figure 8: Acoustic emission waveforms and basic parameters

The acoustic emission signals are categorized into tensile and shear modes, e.g., the results of discriminating the microcracking modes of a specimen during the fracture process are shown in Fig. 9. The calculated critical values of microscopic cracking mode discrimination AR_{lim} for cast and printed specimens are shown in Table 1~Table 2, where n_t and n_s are the respective proportions of the number of tensile and shear microcracks.

According to the results shown in Table 1 to Table 2, we can see that when the content of steel fiber keeps unchanged, the ratio of the number of shear cracks in the printed specimen is higher than that in the cast specimen. This gives us indication that the being of the printed interface brings about an increase in shear cracks, hence specifically those that get formed on the printed interface. In the case where the quantity of steel fibers remains consistent, the percentage of the number of shear cracks in the printed specimens increases sequentially in the order of PP3, CP1, and PP1, which is consistent with the order of weakening of the material integrity of the sections of PP3, CP1, and PP1 specimens. The analysis in this paper suggests that with the weakening of the integrity of the printed material, the number of shear cracks generated during fracture damage increases, i.e., the cracks generated at the material defects. In addition, for each group of printed specimens, the percentage of shear cracks also increases when the steel fiber content increases, which is analyzed to be caused by bond-slip damage at more steel fiber-concrete interfaces due to the increase in steel fiber content.

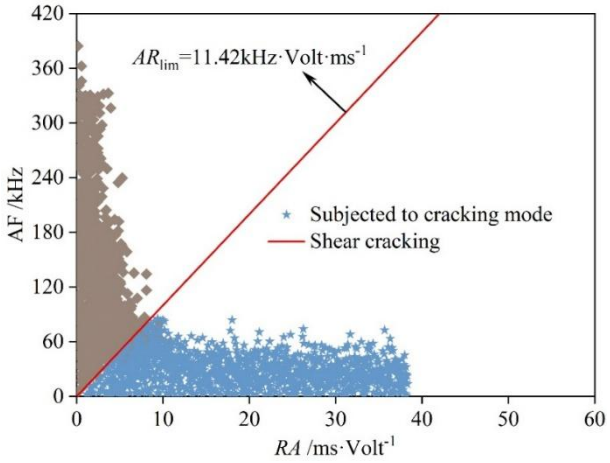

Figure 9: Discrimination results of microscopic crack cracking patterns

Table 1: Classification results of cracking patterns of cast specimens

M_f %	$AR_{\lim}$ /kHz×Volt×ms^{-1}	n_t	n_s
0	12.08	0.94	0.09
0.39	8.13	0.93	0.10
0.95	10.29	0.90	0.14
1.87	7.31	0.88	0.16

Table 2: Classification results of printed specimens cracking modes

Group	M_f %	$AR_{\lim}$ /kHz×Volt×ms^{-1}		n_t		n_s	
		1-axis	3-axis	1-axis	3-axis	1-axis	3-axis
PP	0	8.14	14.29	0.81	0.92	0.25	0.12
	0.39	16.27	13.52	0.78	0.90	0.27	0.14
	0.95	6.63	9.94	0.72	0.88	0.32	0.16
	1.87	7.82	11.45	0.68	0.85	0.38	0.19
CP	0	14.05	-	0.89	-	0.15	-
	0.39	14.91	-	0.88	-	0.16	-
	0.95	17.16	-	0.86	-	0.18	-
	1.87	14.34	-	0.82	-	0.21	-

For inspecting the connection between the macro mechanics performance of the molded samples and the micro crack characteristics in the breaking process, the damping coefficients of every group of molded samples were calculated through the below formula:

$$\mu_f = \frac{f_{f,cast,M_f} - f_{f,print,M_f}}{f_{f,cast,M_f}} \tag{37}$$

$$\mu_G = \frac{G_{f,cast,M_f} - G_{f,print,M_f}}{G_{f,cast,M_f}} \tag{38}$$

$$\mu_{shear} = r_{f,print,M_f} - r_{f,cast,M_f} \tag{39}$$

where μ_f, μ_G and μ_{shear} are the attenuation coefficients for the flexural strength, fracture energy and shear crack percentage of the printed specimen, respectively, and $f_{f,cast,M_f}\left(f_{f,print,M_f}\right)$, $G_{f,cast,M_f}\left(G_{f,print,M_f}\right)$ and $r_{f,cast,M_f}\left(r_{f,print,M_f}\right)$ are the flexural strength, fracture energy, and percentage of shear microcracks in conventionally cast concrete (printed steel fiber concrete) with different fiber contents, respectively.

The $\mu_{shear} - \mu_f$ and $\mu_{shear} - \mu_G$ tests and fitting results are shown in Fig. 10's (a)~(b). When the content of steel fibers is zero, μ_f and μ_G are approximately linearly related to μ_{shear}, but after the addition of steel fibers, μ_f and μ_G show a significantly non-linear relationship with μ_{shear}.

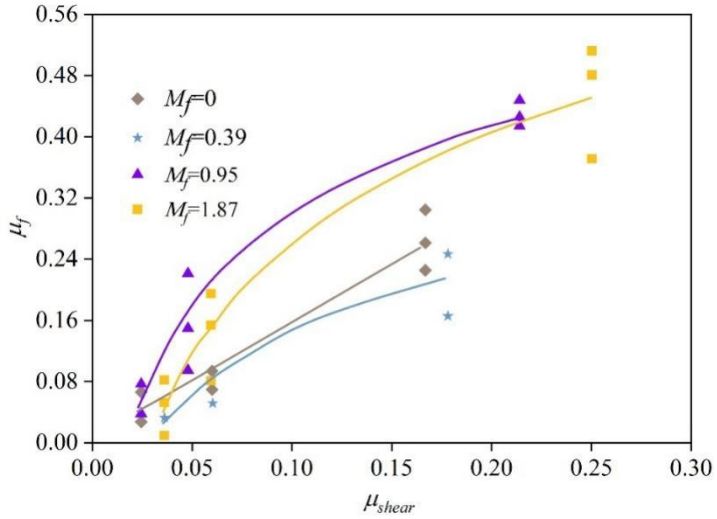

(a) $\mu_{shear} - \mu_f$

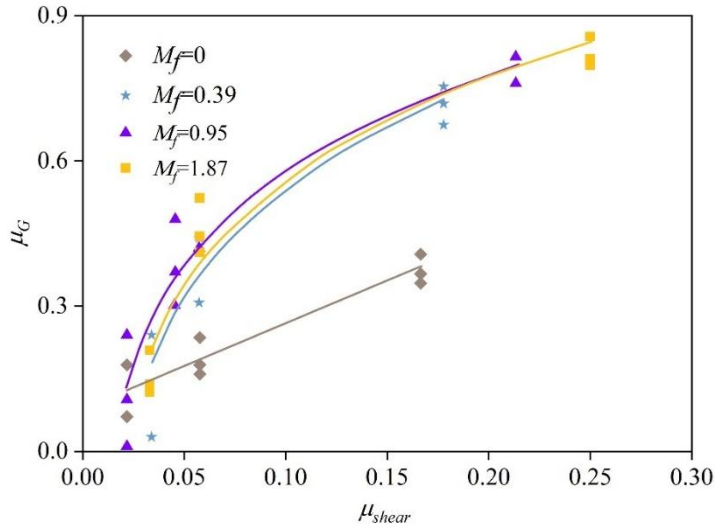

(b) $\mu_{shear} - \mu_G$

Figure 10: The test results and fitting relationships between μ_f, μ_G *and* μ_{shear}

The analysis got the conclusion that when there is no steel fiber content, the material's wholeness is the main factor which affects the macroscopic mechanics performance. On the opposite side, when steel fibers get added, the number of shear cracks which come from bond-slip at the interface between fiber and concrete is to a certain extent not predictable, therefore this is caused by the random distribution of the fibers, resulting in a non-linear correlation between the μ_f, μ_G both with μ_{shear} are nonlinear. The fitting expression is:

$$\mu_F = \begin{cases} a\mu_{shear} + b & M_f = 0 \\ a\ln\mu_{shear} + b & M_f \neq 0 \end{cases} \tag{40}$$

where μ_F denotes μ_f or μ_G. The statistics of parameters a and b are shown in Table 3.

Table 3: The statistical results of parameters a and b

Coefficient	M_f %	*a*	*b*	R^{2t}
μ_f	0	1.92	-0.002	0.985
	0.39	0.14	0.451	0.907
	0.95	0.19	0.728	0.961
	1.87	0.24	0.787	0.932
μ_G	0	2.07	0.076	0.911
	0.39	0.35	1.375	0.914
	0.95	0.32	1.294	0.930
	1.87	0.35	1.363	0.942

According to Eq. (40), the degree that the flexural intensity and fracture energy of printing steel-fiber concrete are lowered when compared with casting steel-fiber concrete can be assessed through keeping record of the percentage of shearing microcracks.

3.2 Numerical simulation results and analysis

In this section, we carry out numerical simulation analysis through the ABAQUS software. This analysis is carried out on the basis of the already built intrinsic model, the cohesive crack model, and the finite-element model.

3.2.1 Comparison of Load-Tension Displacement Characteristic Curves

The properties of the model materials for each control group are shown in Table 4, with a uniform Poisson's ratio of 0.3. where A1 denotes plain concrete, A2 to A4 denote concrete mixed with 0.2% polyvinyl alcohol (PVA), 1.6% ordinary steel fibers, and 1.6% ultrafine steel fibers, respectively, and A5 denotes multifiber concrete mixed with all three materials simultaneously at the ratio of 0.2%, 0.8%, and 0.8%.

Table 4: Properties of concrete materials with different proportions

Group	Compressive strength /MPa	Tensile strength /MPa	Elastic modulus /MPa	Fracture energy /(N·m^{-1})
A1	60.8	3.6	3.54×10^4	351
A2	63.7	3.7	3.57×10^4	417
A3	67.5	3.8	3.86×10^4	5124
A4	74.9	4.2	3.95×10^4	5735
A5	76.8	4.4	3.92×10^4	6053

The comparison of five sets of concrete beam load-tension displacement (P-CMOD) curves simulated by ABAQUS software with the actual specimen loading curves is shown in Fig. 11. Among them, (a) ~ (e) denote the concrete materials A1~A5, respectively.

The comparison shows that the software simulation curve can fit the actual loading curve better. The trend of the curve is roughly divided into 3 stages:

(1) Straight line rising stage, the load value in this stage is less than the crack initiation load, and the cracks have not begun to expand.

(2) Rising curve stage, the load value exceeds the crack initiation load, and the crack begins to expand steadily upward.

(3) Curve descending stage, the load value exceeds the destabilizing load at this stage, and the crack begins to expand rapidly away from the original direction until the crack runs through

the whole specimen.

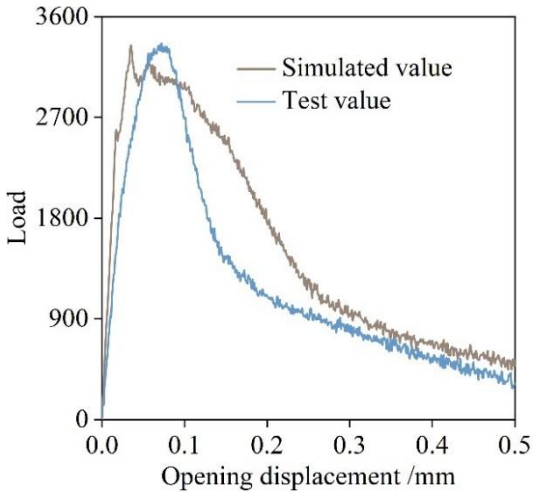

(a) A1

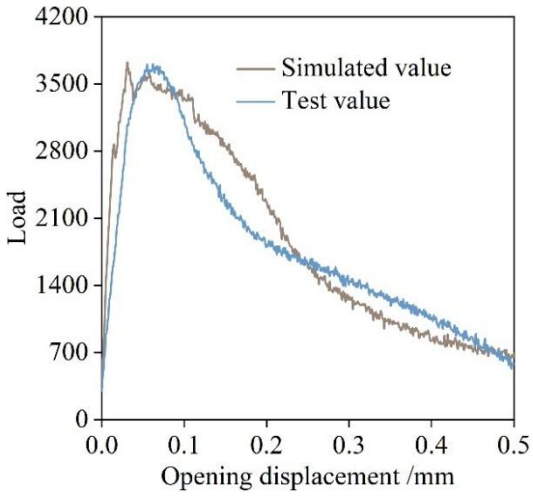

(b) A2

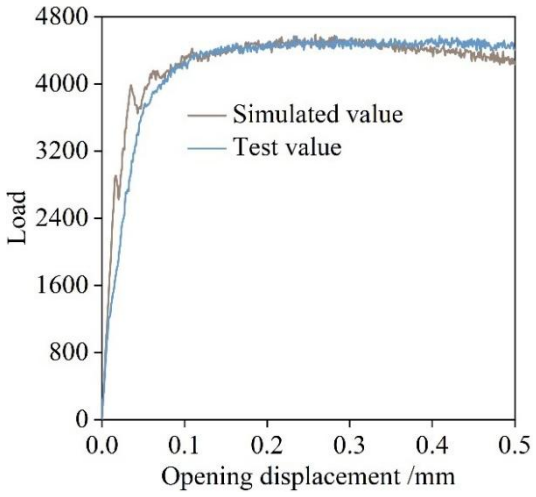

(c) A3

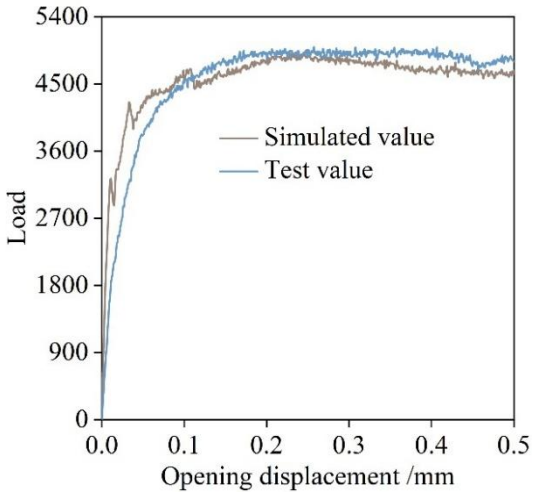

(d) A4

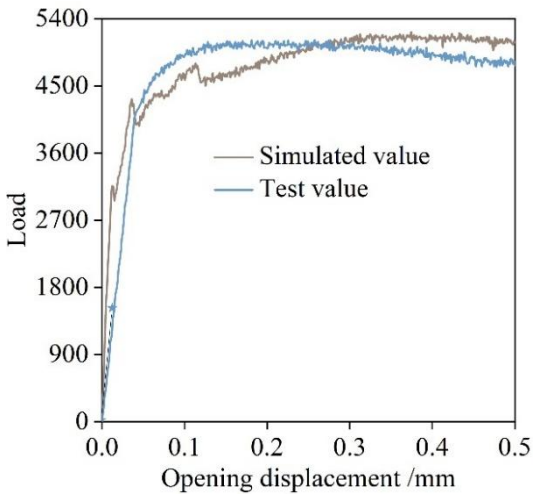

(e) A5

Figure 11: Comparison of load-crack opening displacement curves

3.2.2 Comparison of fracture parameters

After the load-tension-displacement (P-CMOD) curves were simulated by ABAQUS, Origin software was used to determine the initiation load P_{ini} and the critical load F_Q ,The critical load value was then inserted into the fracture toughness equation to compute the fracture toughness K_{IC} . Table 5 shows a comparison of fracture parameter values which were got by simulation through the software and the measured values for each group of test specimens.

It can be seen that the errors of the starting load P_{ini} , critical load F_Q and fracture toughness obtained from the three-point bending beam test simulated by the Abaqus software with the experimental values are not more than 8%, in which the errors of the simulated values of the most important fracture parameter K_{IC} and the experimental values are basically within 4%, and the error of the ternary mixed-fiber group A5 is 7.64%>4%. is 7.64%>4%. The reason for the error may be due to the software in the simulation of concrete specimens as a homogeneous continuum, while the actual concrete materials, especially the ternary hybrid fiber concrete materials, have a complex internal structure, and the fiber dispersion is not completely uniform.

Table 5: Comparison of fracture parameters

Parameter	Control group	A1	A2	A3	A4	A5
Cracking load	Test value /N	2765	3289	3842	3928	4435
	Simulated value /N	2624	3193	4076	4227	4509
	Error /%	5.10	2.92	6.09	7.61	1.67
Critical load	Test value /N	3275	3.794	4306	4528	4937
	Simulated value /N	3238	3.843	4169	4491	4552
	Error /%	1.13	-1.29	3.18	0.82	7.80
Fracture toughness	Test value /(kN·m$^{-3/2}$)	1105.63	1213.48	1395.74	1462.98	1604.62
	Simulated value /(kN·m$^{-3/2}$)	1098.51	1229.36	1347.85	1441.52	1482.07
	Error /%	0.64	1.31	3.43	1.47	7.64

3.2.3 Change in crack length when specimen is loaded

In the process of actual load application upon concrete test pieces, the expansion of cracks takes place with an extremely high speed. To capture the correlation which is among crack length, time, and the loading point's displacement hence proves that it is quite a challenging task. On the opposite side, when we carry out simulation work on the cracking behavior that concrete has, the extended finite-element method is able to carry out continuous monitoring on the extension situation of cracks. It also has the capability to accurately fix the position of the cracks. By this way, the relational connections between the crack length and time, and also between the crack length and the displacement of the loading point, can be gotten.

The variation curves of crack extension height with loading time and loading point displacement for each group of concrete specimens simulated by the software are shown in Fig. 12 (a)~(b), respectively. The time duration in the figure is set at 1, and no unit is specified. Evidently, the fractures in plain concrete and concrete specimens containing a small quantity of PVA fibers expanded at a rapid pace and traversed the entire specimen. In contrast, the cracks in concrete specimens with steel fibers or ternary hybrid fibers expanded gradually until they reached the top of the specimen.

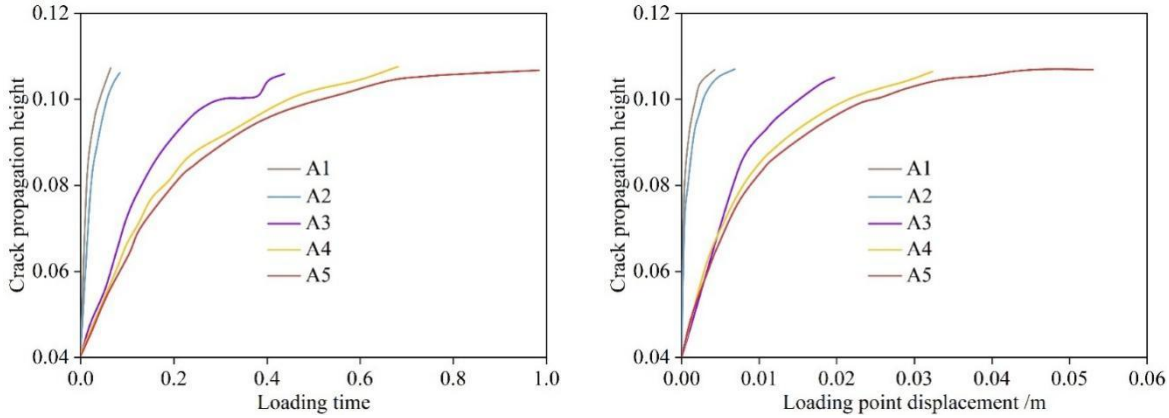

(a) The height of crack propagation varies with the loading time

(b) The height of crack propagation varies with the displacement of the loading point

Figure 12: Curves of crack length change

Table 6 shows the length of loading and the displacement of the loading point at the time when the crack has gone across the test piece. Under this background, the gain ratio is the proportion that the index values of specimens A2 to A5 hold, compared with the index value of specimen A1. The data make known that the time which is taken by the crack for penetrating the 0.2% volume-fraction PVA fiber concrete specimen has increased by 41.79% when making a comparison with the plain concrete. Regarding the concrete test specimens which have 1.6% volume fraction and contain single common steel fiber or ultrafine steel fiber, the times of crack penetration have respectively increased by 505.97% and 807.46%. In these specimens, the specimen of ternary mixed fiber concrete needed the longest time to let cracks penetrate completely, hence it showed an increase of 1231.34% when compared with plain concrete.In terms of the displacement of the loading point during crack penetration, the displacement of the loading point of 0.2% by volume PVA fiber concrete, 1.6% by volume ordinary steel fiber concrete, ultrafine steel fiber concrete, and ternary hybrid fiber concrete specimens increased by 52.53%, 374.07%, 606.56%, and 1033.51%, respectively, as compared to that of plain concrete specimens. It is evident that during crack penetration, ternary hybrid fiber concrete exhibits the greatest capacity to accommodate deformation. After that comes ultrafine steel fiber concrete, then ordinary steel fiber concrete. Among all the groups of fiber concrete, PVA fiber concrete has the relatively weakest ability to adapt to deformation. Nevertheless, compared to plain concrete, its deformation - adaptation ability has also been enhanced.

Table 6: Time of crack penetration specimens and displacements of loading point

Group	A1	A2	A3	A4	A5
Loading time	0.067	0.095	0.406	0.608	0.892
Gain ratio /%	0	141.79	605.97	907.46	1331.34
Loading point displacement /mm	4.053	6.182	19.214	28.637	45.941
Gain ratio /%	0	152.53	474.07	706.56	1133.51

3.3 Fracture energy calculation results and analysis of influencing factors

For carrying out a deeper exploration on the anti-fracture performance and fracture toughness of high-performance steel-fiber concrete, 36 steel-fiber concrete test pieces are selected in this section to carry out an experimental research. The objective is to carry out calculation of their fracture energy and carry out inspection of the factors which exert influence on it.

According to the outcomes from the deep perspective analysis, Table 7 displays the fracture energy and the increment of fracture energy for every group of steel fiber concrete three-point bending test samples. This data has relation to a condition that the volume percentage of steel fiber is 1.6%. Where specimen number C30-XX-ZZ, C30 denotes the concrete strength grade, XX denotes the maximum coarse aggregate particle size $D_{\max}$ (mm), and ZZ denotes the steel fiber length L_f (mm).

Table 7: Calculation results of fracture energy of C30 steel fiber reinforced concrete

Specimen number	Breaking energy /(N·m^{-1})	Gain ratio	Specimen number	Breaking energy /(N·m^{-1})	Gain ratio
C30-10	133.70	1	C30-20-70	3199.61	19.35
C30-20	165.34	1	C30-20-80	2915.79	17.64
C30-30	205.97	1	C30-30-10	2431.85	11.81
C30-40	192.33	1	C30-30-20	2890.71	14.03
C30-10-10	1887.16	14.11	C30-30-30	3165.14	15.37
C30-10-20	2101.15	15.72	C30-30-40	3450.87	16.75
C30-10-30	2316.91	17.33	C30-30-50	3885.67	18.87
C30-10-40	2483.55	18.58	C30-30-60	4295.65	20.86
C30-10-50	2690.45	20.12	C30-30-70	3804.44	18.47
C30-10-60	2725.62	20.39	C30-30-80	3574.94	17.36
C30-10-70	2536.49	18.97	C30-40-10	2236.57	11.63
C30-10-80	2198.74	16.45	C30-40-20	2749.55	14.30
C30-20-10	2054.93	12.43	C30-40-30	2910.63	15.13
C30-20-20	2289.89	13.85	C30-40-40	3214.21	16.71
C30-20-30	2477.04	14.98	C30-40-50	3589.29	18.66
C30-20-40	2563.46	15.50	C30-40-60	3840.68	19.97
C30-20-50	3164.44	19.14	C30-40-70	3658.02	19.02
C30-20-60	3416.21	20.66	C30-40-80	3432.41	17.85

3.3.1 Effect of coarse aggregate particle size

According to what Table 7 shows, the relation among fracture energy, the ratio of fracture energy increment in steel fiber-reinforced concrete, and the maximum grain size of coarse aggregate ($D_{\max}$) has been set up.The graphical representation of this relationship is presented in Figures 13 through 14. The size of bubbles in the figure indicates the length of steel fiber.

It is obvious that, when steel fibers have a certain fixed length, the fracture energy of steel-fiber concrete and its growth ratio, as the maximum size of coarse aggregate particles becomes larger, generally first go up and then go down.This occurs because the coarse aggregate not only acts as an impediment to crack propagation but also lessens the impact stemming from the existence of initial cracks at the boundary between the aggregate and the mortar. Furthermore, the fracture energy of concrete which is reinforced by steel fibers reaches its maximum when the maximum size of particles of the coarse aggregate is 30 mm. After the particle dimension of the coarse aggregate increases to a certain extent, the original cracks at the boundary between the coarse aggregate and the mortar become more in quantity. This, as a result, makes the intensity of the connection between thick gathering stuff and the matrix concrete become weaker. Therefore, the fracture energy of the concrete which is reinforced by steel fibers has a decrease.

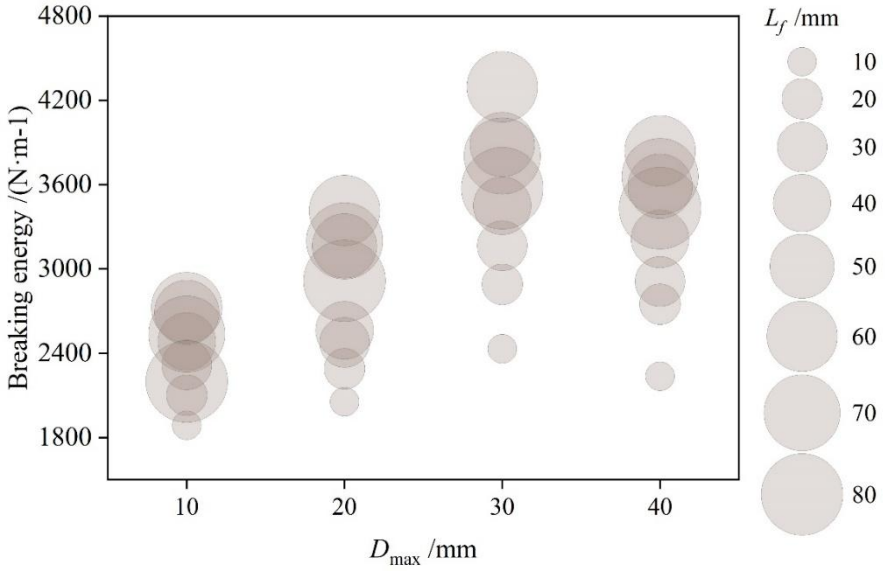

Figure 13: The relationship between fracture energy and the D_{max}

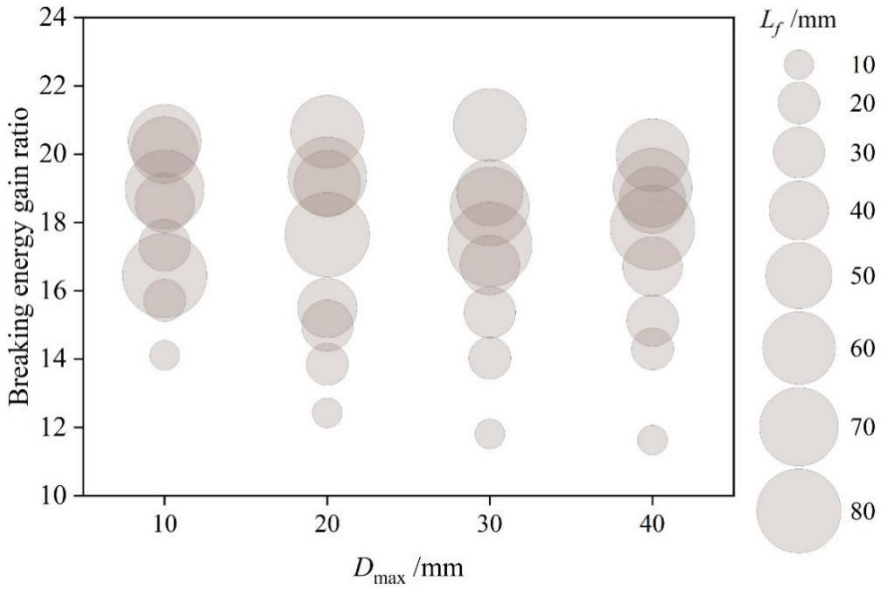

Figure 14: The relationship between the fracture energy gain ratio and the D_{max}

3.3.2 Effect of steel fiber length

Similarly, based on the data plotted in Table 7, the relationship between the fracture energy and fracture energy gain ratio of steel fiber concrete and the length of steel fiber (L_f) is obtained as shown in Figures 15 to 16.

It is very clear that when the length of steel fibers becomes longer, the fracture energy of steel fiber-reinforced concrete and its gain ratio first go up and then go down. The peak numerical magnitudes are obtained when the length of the steel fibers attains 60 mm. This kind of situation happens because when the length of steel fibers becomes bigger, the anchoring function of steel fibers inside concrete is getting enhancement. Therefore, this makes the combining power between steel fibers and concrete become stronger, thus effectively holding

back the expanding process of cracks.Nevertheless, when the length of steel fibers arrives at a certain degree, the number of steel fibers under a fixed volume fraction becomes lower. Furthermore, in the process of mixing, the steel fibers have probability to be bent. This brings down the effective direction coefficient of steel fibers, hence, the fracture energy of steel fiber-reinforced concrete is thus made smaller.

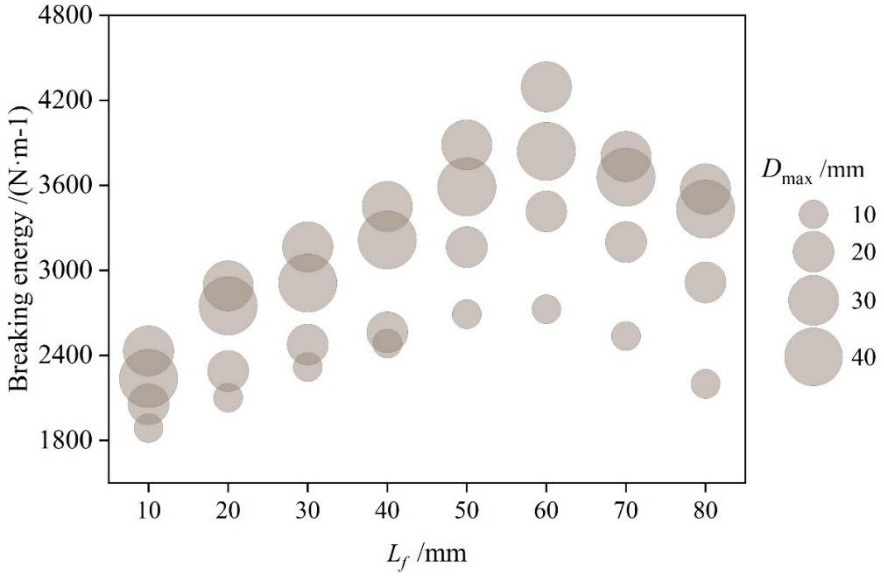

Figure 15: The relationship between fracture energy and the L_f

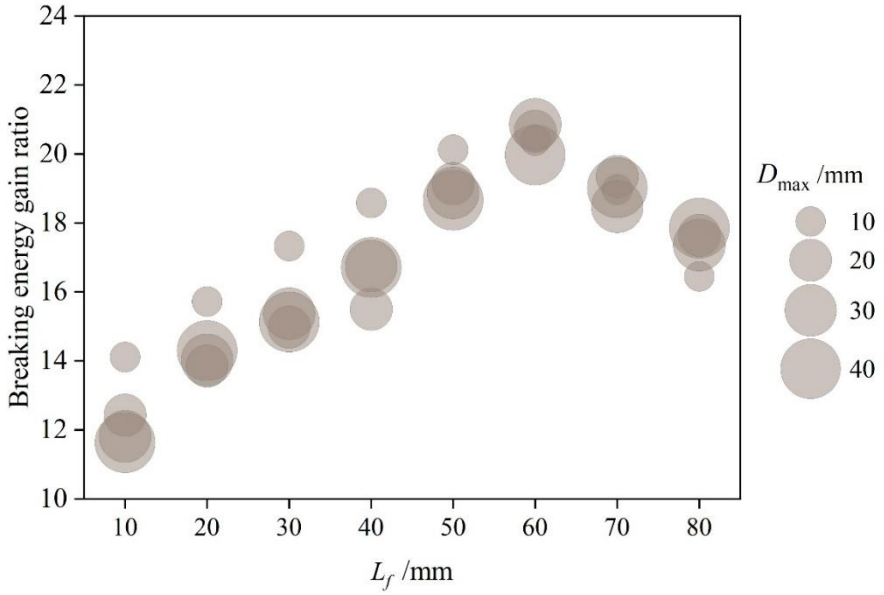

Figure 16: The relationship between the fracture energy gain ratio and the L_f

3.3.3 Coupling of coarse aggregate particle size and steel fiber length

Based on the aforementioned calculation outcomes, the dispersion of steel fibers within concrete is influenced by the grain size of coarse aggregate. In addition, a suitable mixing of the length of steel fibers and the grain size of coarse aggregate can greatly enhance the fracture performance of steel fiber-reinforced concrete. In various maximum particle diameter ranges of coarse aggregate, the trend of the fracture energy gain ratio of steel fiber concrete with the

ratio of steel fiber length and maximum particle size of coarse aggregate L_f/D_{max} is shown in Fig. 17.

It is observable that the gain ratio of fracture energy in steel fiber - reinforced concrete initially rises and subsequently declines as L_f / D_{max} increases. When D_{max} is 10mm and 20mm, the fracture energy gain ratio reaches its maximum at $L_f / D_{max} = 3$, with an increase of 46.42%. When D_{max} =30mm and 40mm, the fracture energy gain ratio reaches its maximum at $L_f / D_{max} = 2$, with an increase of 79.36%. Within the range of this calculation, for concrete with D_{max} =10mm and 20mm, when L_f / D_{max} =2.5~7, the effect of steel fibers on the fracture energy of concrete is better. For concrete with D_{max} =30mm and 40mm, when L_f / D_{max} =1.25 to 2.67,the influence that steel fibers exert upon the fracture energy of concrete is more advantageous.

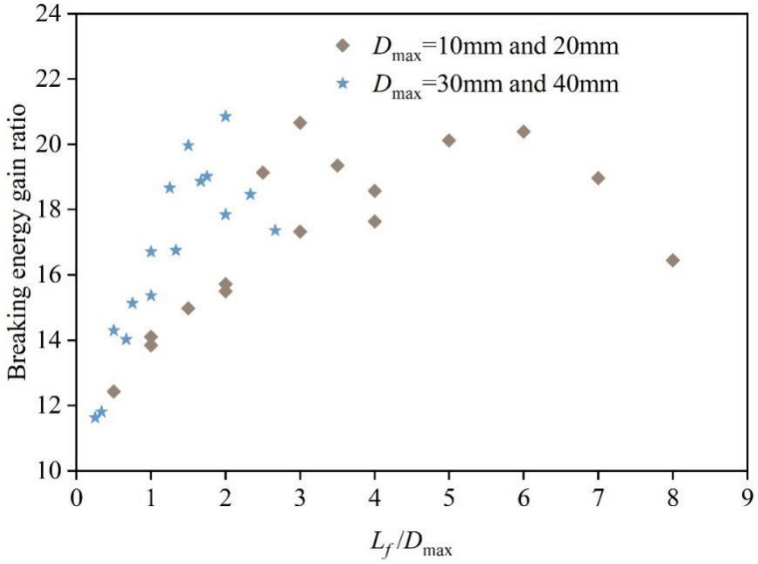

Figure 17: The relationship between the breaking energy gain ratio and L_f/D_{max}

3.3.4 Effect of Steel Fiber Volumetric Ratio

Taking consideration of the foregoing calculation outcomes and the requirement for large dimension aggregate materials in hydropower engineering projects, this section investigates the influence of the steel fiber volume proportion on the breaking energy of steel-fiber-reinforced concrete. This evaluation is conducted under the situation that the maximum dimension of the coarse aggregate is 20 mm and the length of the steel fiber is 40 mm. Table 8 gives the break energy of steel-fiber-reinforced concrete which corresponds to different volume portions of steel fiber.

When the dimension of the big-sized aggregate is 20 mm and the length of the steel fiber is 40 mm, it is very clear that the fracture energy of steel fiber-reinforced concrete at first increases and after that drops as the volume fraction of steel fibers becomes larger. To speak specifically, it reaches its highest value when the volume percentage of steel fibers is 1.6%. The cause of the early rising of fracture energy is as follows: When the volume proportion of steel fibers increases, these fibers which are inside the concrete act as bridging components. When cracks start to generate, the existence of these steel fibers makes it necessary that more energy be absorbed.This additional energy absorption is necessary to overcome the resistance provided by the steel fibers, hence promoting the fracture energy of the concrete which is reinforced by

steel fiber. From another aspect, when the volume ratio of steel fibers is relatively high, hence the steel fibers have a tendency to gather together. This kind of gathering phenomenon brings disturbance to the even placing of steel fibers inside the concrete. Therefore, the ability that steel fibers have to effectively promote the concrete's fracture resistance ability is reduced, hence causing a lowering of the fracture energy of the steel fiber-reinforced concrete.

Table 8: Fracture energy of steel fiber reinforced concrete under different volume ratios

Volume ratio of steel fibers ρ_f	0.4%	1.0%	1.6%	2.2%
Breaking energy /(N·m^{-1})	1931.17	2563.46	2886.84	2108.09
Gain ratio	11.68	15.50	17.46	12.75

4 Conclusion

In this research paper, we have carried out an investigation on the capability of high-performance steel fiber concrete to bear fractures and cracks. For the completion of this research, a three-dimensional model of the high-performance steel fiber concrete was established through the utilization of the ABAQUS finite element software. The main research results of this study are following:

(1) The greater weakening of material integrity is microscopically reflected in the increase in the percentage of the number of shear cracks in the fracture process. When steel fibers are not incorporated, the attenuation coefficient of the percentage of shear cracks μ_{shear} and the attenuation coefficient of the fracture mechanical properties μ_f and μ_G are all linearly related, whereas, when steel fibers are incorporated, then due to the randomness of the distribution of the fibers, the μ_{shear} has a nonlinear relationship with μ_f and μ_G.

(2) Different types of fiber concretes exhibit significant differences in fracture toughness at conventional fiber admixture. Steel-fiber concrete and ternary fiber blends exhibited better fracture resistance and toughness relative to plain concrete and PVA fiber concrete with 0.16% volume admixture.

(3) The expanded finite-element method has the ability to carry out continuous monitoring on the position of cracks.Therefore, it can help us to establish the correlative relation among the crack length, the loading time, and the displacement which is at the loading point. In the process of numerical simulation calculation works, the speeds of crack expansion have differences among the different groups of concrete test samples. To speak specifically, the crack expanding speed of common concrete was obviously bigger than that of the fiber-strengthened concrete. If we say it more exactly, the crack expanding speed of common concrete was about 1.4 - 1.6 times that of PVA fiber-strengthened concrete with 0.16% volume mixing amount, 6 - 9 times that of steel fiber-strengthened concrete with 1.6% volume mixing amount, and 11 - 14 times that of three-element mixed fiber-strengthened concrete.

(4) When the maximum dimension of the coarse aggregate and the length of the steel fibers got increased, the fracture energy of the steel fiber-reinforced concrete and its increase proportion first went up and then went down. The maximum numerical values were obtained when the maximum dimension of the coarse aggregate was 30 mm and the length dimension of the steel fibers was 60 mm.

(5) In the research field which this paper belongs to, when the maximum size of coarse aggregate particles is 20 millimeters, the length of steel fiber is 40 millimeters, and the volume percentage of steel fiber is 1.6%, the enhancement effect of steel fiber on concrete is relatively more good. The formulation of steel-fiber-reinforced concrete may be carried out according to

this matching method to satisfy the demand for the application of large-particle-size steel-fiber-reinforced concrete in hydraulic engineering structures.

About the Author

Cuijin Wang was born in Taiyuan, Shanxi, P.R. China, in 1990. She obtained a master's degree from Dalian University of technology in China. She is currently working at the Department of Civil and Environmental Engineering, Chengdu Jincheng College. Her main research direction is Analysis of concrete fracture performance.

References

[1] Anas, M., Khan, M., Bilal, H., Jadoon, S., & Khan, M. N. (2022). Fiber reinforced concrete: a review. Engineering Proceedings, 22(1), 3.

[2] Akbulut, Z. F., Tawfik, T. A., Smarzewski, P., & Guler, S. (2025). Advancing Hybrid Fiber-Reinforced Concrete: Performance, Crack Resistance Mechanism, and Future Innovations. Buildings, 15(8), 1247.

[3] Shafei, B., Kazemian, M., Dopko, M., & Najimi, M. (2021). State-of-the-art review of capabilities and limitations of polymer and glass fibers used for fiber-reinforced concrete. Materials, 14(2), 409.

[4] Chu, S. H., Li, L. G., & Kwan, A. K. H. (2021). Development of extrudable high strength fiber reinforced concrete incorporating nano calcium carbonate. Additive Manufacturing, 37, 101617.

[5] Abbass, W., Khan, M. I., & Mourad, S. (2018). Evaluation of mechanical properties of steel fiber reinforced concrete with different strengths of concrete. Construction and building materials, 168, 556-569.

[6] Niu, Y., Wei, J., & Jiao, C. (2021). Crack propagation behavior of ultra-high-performance concrete (UHPC) reinforced with hybrid steel fibers under flexural loading. Construction and Building Materials, 294, 123510.

[7] Yao, X., Lu, M., Guan, J., Han, A., Wang, H., Li, L., ... & He, S. (2022). Development of a design method for the fracture performance of steel fiber-reinforced concrete by considering steel fiber characteristics and aggregate gradation. Theoretical and Applied Fracture Mechanics, 121, 103486.

[8] Luo, X., Sun, W., & Chan, S. Y. N. (2001). Steel fiber reinforced high-performance concrete: a study on the mechanical properties and resistance against impact. Materials and Structures, 34(3), 144-149.

[9] Devi, C., Vijayan, D. S., Nagalingam, R., & Arvindan, S. (2022). A review of the implementations of glass fiber in concrete technology. Materials Today: Proceedings, 62, 2010-2015.

[10] Wu, C., He, X., Zhao, X., He, L., Song, Y., & Zhang, X. (2022). Effect of fiber content

on mechanical properties and microstructural characteristics of alkali resistant glass fiber reinforced concrete. Advances in Materials Science and Engineering, 2022(1), 1531570.

[11] Aliha, M. R. M., reza Karimi, H., & Abedi, M. (2022). The role of mix design and short glass fiber content on mode-I cracking characteristics of polymer concrete. Construction and Building Materials, 317, 126139.

[12] Xiaochun, Q., Xiaoming, L., & Xiaopei, C. (2017). The applicability of alkaline-resistant glass fiber in cement mortar of road pavement: Corrosion mechanism and performance analysis. International Journal of Pavement Research and Technology, 10(6), 536-544.

[13] Zhang, C., Zhu, Z., Wang, S., & Zhang, J. (2023). Macro-micro mechanical properties and reinforcement mechanism of alkali-resistant glass fiber-reinforced concrete under alkaline environments. Construction and Building Materials, 368, 130365.

[14] Ruben, N., Venkatesh, C., Durga, C. S. S., & Chand, M. S. R. (2021). Comprehensive study on performance of glass fibers-based concrete. Innovative Infrastructure Solutions, 6(2), 112.

[15] Latifi, M. R., Biricik, Ö., & Mardani Aghabaglou, A. (2022). Effect of the addition of polypropylene fiber on concrete properties. Journal of Adhesion Science and Technology, 36(4), 345-369.

[16] Liu, Y., Wang, L., Cao, K., & Sun, L. (2021). Review on the durability of polypropylene fibre‐reinforced concrete. Advances in Civil Engineering, 2021(1), 6652077.

[17] Qin, Y., Zhang, X., Chai, J., Xu, Z., & Li, S. (2019). Experimental study of compressive behavior of polypropylene-fiber-reinforced and polypropylene-fiber-fabric-reinforced concrete. Construction and Building Materials, 194, 216-225.

[18] Alsadey, S., & Salem, M. (2016). Influence of polypropylene fiber on strength of concrete. Am. J. Eng. Res, 5(7), 223-226.

[19] Ibrahim, Y. A., Hasan, A. H., & Maroof, N. R. (2019). Effects of polypropylene fiber content on strength and workability properties of concrete. Polytechnic Journal, 9(1), 3.

[20] Krishna, N. K., Prasanth, M., Gowtham, R., Karthic, S., & Mini, K. M. (2018). Enhancement of properties of concrete using natural fibers. Materials Today: Proceedings, 5(11), 23816-23823.

[21] Islam, M. S., & Ahmed, S. J. (2018). Influence of jute fiber on concrete properties. Construction and Building Materials, 189, 768-776.

[22] Ahmadi, M., Farzin, S., Hassani, A., & Motamedi, M. (2017). Mechanical properties of the concrete containing recycled fibers and aggregates. Construction and Building Materials, 144, 392-398.

[23] Geremew, A., De Winne, P., Demissie, T. A., & De Backer, H. (2021). Treatment of natural fiber for application in concrete pavement. Advances in Civil Engineering, 2021(1), 6667965.

[24] Ahmad, J., Arbili, M. M., Majdi, A., Althoey, F., Farouk Deifalla, A., & Rahmawati, C. (2022). Performance of concrete reinforced with jute fibers (natural fibers): A review. Journal of Engineered Fibers and Fabrics, 17, 15589250221121871.

[25] Yinh, S., Hussain, Q., Joyklad, P., Chaimahawan, P., Rattanapitikon, W., Limkatanyu, S., & Pimanmas, A. (2021). Strengthening effect of natural fiber reinforced polymer composites (NFRP) on concrete. Case Studies in Construction Materials, 15, e00653.

[26] John, V. J., & Dharmar, B. (2021). Influence of basalt fibers on the mechanical behavior of concrete—A review. Structural Concrete, 22(1), 491-502.

[27] Zhou, H., Jia, B., Huang, H., & Mou, Y. (2020). Experimental study on basic mechanical properties of basalt fiber reinforced concrete. Materials, 13(6), 1362.

[28] Branston, J., Das, S., Kenno, S. Y., & Taylor, C. (2016). Mechanical behaviour of basalt fibre reinforced concrete. Construction and Building Materials, 124, 878-886.

[29] Jalasutram, S., Sahoo, D. R., & Matsagar, V. (2017). Experimental investigation of the mechanical properties of basalt fiber‐reinforced concrete. Structural Concrete, 18(2), 292-302.

[30] Khan, M., Cao, M., Xie, C., & Ali, M. (2022). Hybrid fiber concrete with different basalt fiber length and content. Structural Concrete, 23(1), 346-364.